Biomicrofluidics ARTICLE scitation.org/journal/bmf

Rheological behavior of bimodal distribution emulsions on flow adoptability

Cite as: Biomicrofluidics 13, 014109 (2019); doi: 10.1063/1.5083858
Submitted: 30 November 2018 · Accepted: 21 January 2019 ·
Published Online: 7 February 2019

Jae Yong Park, Se Bin Choi, and Joon Sang Lee[a)]

AFFILIATIONS

Department of Mechanical Engineering, Yonsei University, Seoul 03772, South Korea

[a)]Author to whom correspondence should be addressed: joonlee@yonsei.ac.kr

ABSTRACT

This paper analyzed colloidal characteristics of a bimodal distribution emulsion system using bulk rheological and numerical approaches. The experiment measured simple shear to confirm emulsion shear thinning and viscosity tendencies. Numerical models employed the multi-component lattice Boltzmann method to express interfacial tension, surfactant movement, and viscosity of liquid phases. Numerical models were helpful to implement interactions between two or more varied-sized liquid droplets, since they express droplet deformation and interaction forces and can also provide rheological analysis, whereas shear flow experiments cannot. In monodisperse systems (i.e., uniform droplet size), larger droplets decrease emulsion relative viscosity. However, mixture viscosity for bimodal systems (small droplets mixed with large droplets) was lower than that for the monodisperse system. The reduced viscosity was related to increased droplet deformability and decreased shear stress at the droplet surface.

I. INTRODUCTION

Bimodal size distribution of an emulsion system is commonly observed due to coalescence or droplet breakup. For many practical applications, emulsions of different bimodal size distributions have been found. For example, in oil transportation, petrochemical, food, and cosmetic industries, emulsion environmental or formulation parameters change continuously during manufacturing and storage. The cause of these changes can be easily explained by various factors related to emulsion size distribution, including mechanical factors, e.g., disperser rotation speed causing different shear stress,[1] and chemical factors such as surfactant concentration effects on surface tension[2] or continuous phase pH due to surfactant ionic characteristics.[3]

Bimodal emulsions due to mechanical and chemical influences have unique rheological properties. Previous studies have shown that controlling the size distribution can modify viscosity and shear thinning tendencies,[4–7] with related changes in storage and loss modulus due to modifying the bulk rheology. Although several studies have suggested that the various interactions could differ depending on the emulsion size distribution, the studies were limited to bulk rheology investigations with highly concentrated solutions.

The development of macroscopic rheometric techniques using microfluidic channels has enabled studying the macroscopic environment. For example, droplet coalescence and break up mechanisms could be represented by continuous flow through a microchannel with a varying cross-section area, which allowed interfacial tension conditions to be investigated.[8] Changes in surface tension and surfactant motion for fluorescent surfactants were measured by droplet deformability and mobility,[9] and droplet deformation in simple shear regions has also been investigated in coaxial channels.[10] The surfactant concentration was found to be related to droplet deformability and surface tension, but experimental studies using microfluidic channels limited the available emulsion density range, causing difficulty in observing emulsion interactions.

Microscopic studies have also been conducted using numerical methods. Several studies have employed these methods to analyze interaction forces between droplets, considering emulsions as hard particles. Leba *et al.*[11] modeled homogeneous (consisted of emulsions with same size) spherical emulsion droplets using particle cluster aggregation models to confirm emulsion aggregation. Langevin dynamics were also applied to compare flocculant structures for a

mono-distribution system as a function of emulsion concentration.[12] Zhang *et al.*[13] investigated the probability of coalescence in an electric field for mono-distribution droplets using an interaction force model. However, these interaction models considered the droplets to be hard spheres.

Cristini *et al.*[14] considered deformable droplets and investigated droplet breakup processes under shear stress in extensional flow. Homogenously sized deformable droplets were also considered using a moving surfactant model.[15] However, they could only observe surfactant concentration and flow change near the interface, which are difficult to validate by microscopic experiments.

Figure 1 summarizes the approach taken in the present study. We analyzed emulsion bimodal distribution effects in dilute solutions, which was a major limitation of previous studies.[4–7] To investigate bulk rheology, we made an emulsion droplet solution, estimated the droplet size, and measured the viscosity; and we employed the multi-component lattice Boltzmann method (LBM).[16] To study microscopic rheology, LBM can describe multiple droplets using a surfactant diffusion model under shear flows. We analyzed microscopic fluid flow near the droplet interface, along with droplet arrangements and droplet deformation. Simulation and experimental results were compared using the fine emulsion volume, V_f.

II. METHODS

A. Emulsion fabrication and measurements

Emulsion experiments were optimized based on the simulation environments and solution stability. A relatively stable oil-in-water emulsion was chosen, following Boyd *et al.*[17] using olive oil, deionized water, and glycerol (DAEJUNG Chemicals and Metals Co.). Glycerol was mixed in water at 20 wt. %, with added 2 wt. % Triton X-100 surfactant.

Fine and coarse sized oil-in-water emulsions were prepared (70 ml of each), with the same oil concentration (approximately 29% of volume). This is a common practical concentration[18] and is sufficient to eliminate creaming effects.[19] The emulsion solutions were prepared by bulk stirring with an IKA T-25 homogenizer, as shown in Fig. 2, to produce the desired size distribution. The size distribution for each emulsion is expressed in terms of V_f.

A stress control rheometer (TA instruments DHR-1) was used to perform simple shear tests. Rheology tests were performed using the cone-plate geometry (diameter: 40 mm, angle: 2°), with a plate temperature maintained at 25 °C, and the applied stress was increased linearly as a function of time. Phase contrast microscope images were used to compare emulsion droplet sizes, and all microscope samples were handled

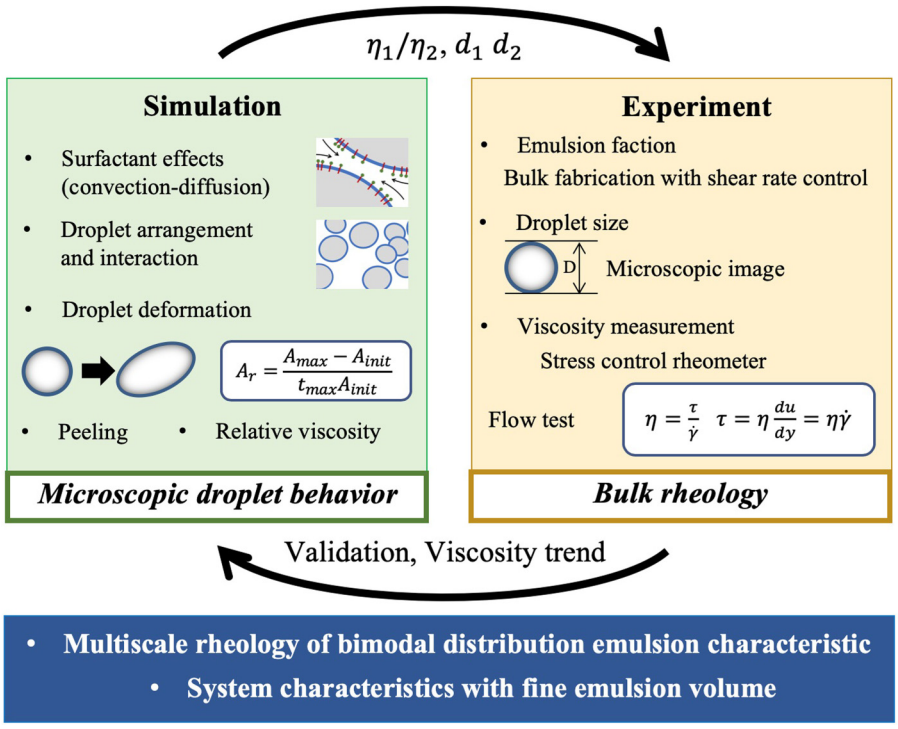

FIG. 1. Current study's objectives.

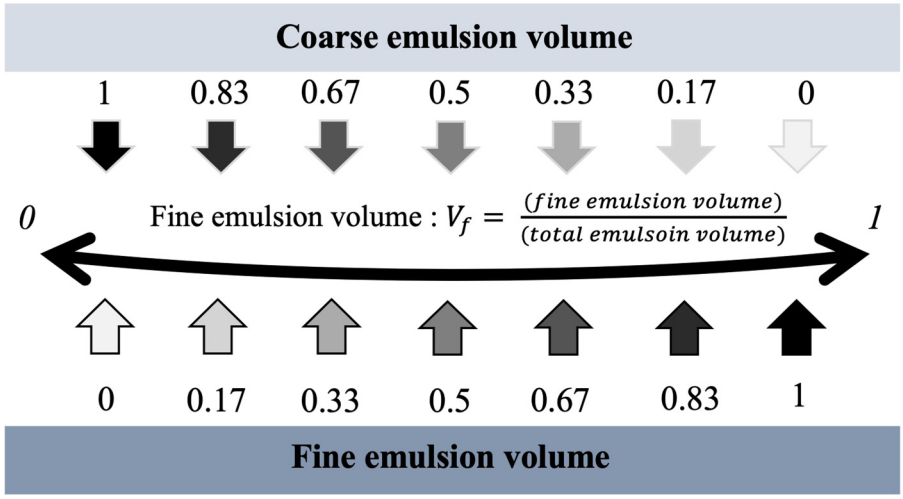

FIG. 2. Seven mixtures made for a specific size distribution. The upper value indicates coarse emulsion volume, and the lower value indicates fine emulsion volume.

and photographed within 3 h. ImageJ® software (U.S. National Institute of Health, Bethesda, MD, USA) was used to estimate emulsion sizes.

B. 3D lattice Boltzmann model for immiscible two-phase fluids

The D3Q19 LBM Gunstensen LBM[16,20–22] was used to simulate two fluid phase systems in an emulsion solution

$$f_i(\mathbf{x} + c_i\delta_t, t + \delta_t) - f_i(\mathbf{x}, t) = -\frac{1}{\tau}[f_i(\mathbf{x}, t) - f_i^{(eq)}(\mathbf{x})] + \phi_i(\mathbf{x}), \quad (1)$$

where f_i is the density distribution function; f_i^{eq} is the equilibrium distribution function; $i = 1,...,19$ denotes the velocity vectors; δ_t and δ_x are the lattice time step and space, respectively; $c = \delta_x/\delta_t = 1$. The speed of sound, $c_s = c/\sqrt{3}$, is applied to calculate fluid pressure $p = \rho c_s^2$ and lattice relaxation time, $\tau = \lambda/\delta$, where λ is the physical relaxation time, and the other parameters are shown in Fig. 3.

Kinetic viscosity and the relaxation time can be expressed as

$$\nu = (\tau - 0.5)\, c_s^2 \delta_t, \quad (2)$$

and Eq. (1) has the equilibrium distribution function

$$f_i^{(eq)} = \rho\omega_i\left[1 + \frac{3}{c^2}\mathbf{c_i}\cdot\mathbf{u} + \frac{9}{2}\frac{(\mathbf{c_i}\cdot\mathbf{u})^2}{c^4} - \frac{3}{2}\frac{\mathbf{u}^2}{c^2}\right], \quad (3)$$

where ω_i is the weighting factor that defines the relative probability of a molecular motion in the ith direction; and ρ and $\mathbf{u}$ are the microscopic density and velocity,

$$\rho = \sum_{i=0}^{Q-1} f_i, \quad \rho\mathbf{u} = \sum_{i=0}^{Q-1} \mathbf{c_i} f_i, \quad (4)$$

respectively, and Q is the number of velocity vectors, dependent on the type of LBM model.

A two-immiscible fluid emulsion was simulated using the Gunstensen model,[16] and the two fluid domains in Fig. 3(b) can be expressed using the following total distribution function:

$$f_i(\mathbf{x}, t) = f_i^R(\mathbf{x}, t) + f_i^B(\mathbf{x}, t), \quad (5)$$

where f_i^R and f_i^B are the red and the blue fluid distribution functions, respectively. The interface between the two fluids can be tracked as[20]

$$\rho^N(\mathbf{x}, t) = \frac{\rho^R(\mathbf{x}, t) - \rho^B(\mathbf{x}, t)}{\rho^R(\mathbf{x}, t) + \rho^B(\mathbf{x}, t)}. \quad (6)$$

The phase field value is in the range $-1 \le \rho^N \le 1$, with $\rho^N \cong 1$ considered to be the inner fluid domain and $\rho^N \cong -1$ is the outer domain. The pressure difference at the interface between the fluids is maintained through surface tension, which is applied with the following macroscopic force:[22]

$$F(x) = -\frac{1}{2}\alpha k \nabla\rho^N, \quad (7)$$

where α is the interfacial tension parameter and k is the interfacial curvature. The model for the relationship between the

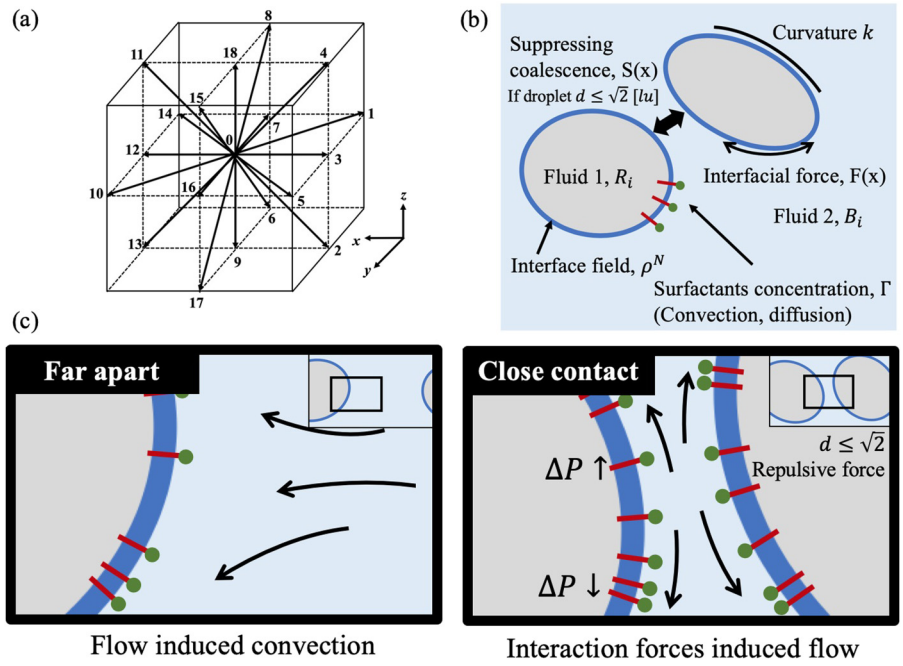

FIG. 3. (a) D3Q19 LBM velocity vectors. (b) A description of the two-immiscible fluid domain, interfacial force, as well as other interactional forces, in a multi-component Gunstensen model,[16] and (c) the movement of surfactant molecules by flow-induced convection and interaction-forces-induced convection.

source term $\phi_i(\mathbf{x})$ and the macroscopic force F(x)[23] can be expressed as

$$\phi_i(\mathbf{x}) = \omega_i\left(1-\frac{1}{2\tau}\right)[3(e_i-u^*)+9(e_iu^*)e_j]F(x) \tag{8}$$

and

$$u^* = \frac{1}{\rho}\left[\sum_{i=0}^{Q-1} f_i e_i + \frac{1}{2}F(x)\right]. \tag{9}$$

where the corrected velocity, u^*, is used to calculate the equilibrium function. This parameter is affected by local interfacial tension, which has mutual influence on the surface tension.

After the collision step, the fluid is segregated[21] into red and blue fluids[20]

$$\bar{\bar{f}}_i^{R}(x, t+\delta_t) = \frac{\rho^R}{\rho^R+\rho^B}\bar{f}_i(x, t+\delta_t) + \beta\frac{\rho^R\rho^B}{\rho^R+\rho^B}\omega_i\cos(\theta_f-\theta_i)|c_i| \tag{10}$$

and

$$\bar{\bar{f}}_i^{B}(x, t+\delta_t) = \bar{f}_i(x, t+\delta_t) - \bar{\bar{f}}_i^{R}(x, t+\delta_t), \tag{11}$$

where $\bar{\bar{f}}_i^{B}$ and $\bar{\bar{f}}_i^{R}$ are the post-collision and the post-segregation distribution functions for the blue and red fluids; $\bar{f}_i$ is the post-collision distribution function; θ_f and θ_i are the polar angle in the color field, and angle of the velocity link, respectively; and β is a segregation parameter.

The droplets tend to interact when they are close to one another. LBM includes the coalescence driving force, which makes droplets to pull each other and eventually merge together. Therefore, a repulsive force was heuristically imposed based on the distance between interfacial nodes, $d \le \sqrt{2}$ [lu], where [lu] is the lattice space unit. The repulsive force is applied as follows:

$$S(x) = c_{in}^*\lambda(\alpha)\alpha(x), \tag{12}$$

where $c_{in}^* = f(c_{in}/c_{in}^{min})$ is the nonlinear function for initial surfactant coverage, c_{in} and minimum coverage ratio, c_{in}^{min}, suppresses coalescence in a particular mixture.[24] The LBM interfacial tension parameter $\lambda(\alpha)$ is a dimensionless nonlinear function $\alpha(x)$. Further details regarding this model can be found in Farhat *et al.*[15]

Figure 3(c) shows an example of near-droplet convection flow. Typically, convection occurs at the interface due to external flow. When they experience the repulsive force, external flow convection is reduced and the interaction force induced convection dominates. Therefore, near-droplet flow variation was modeled following the time-dependent

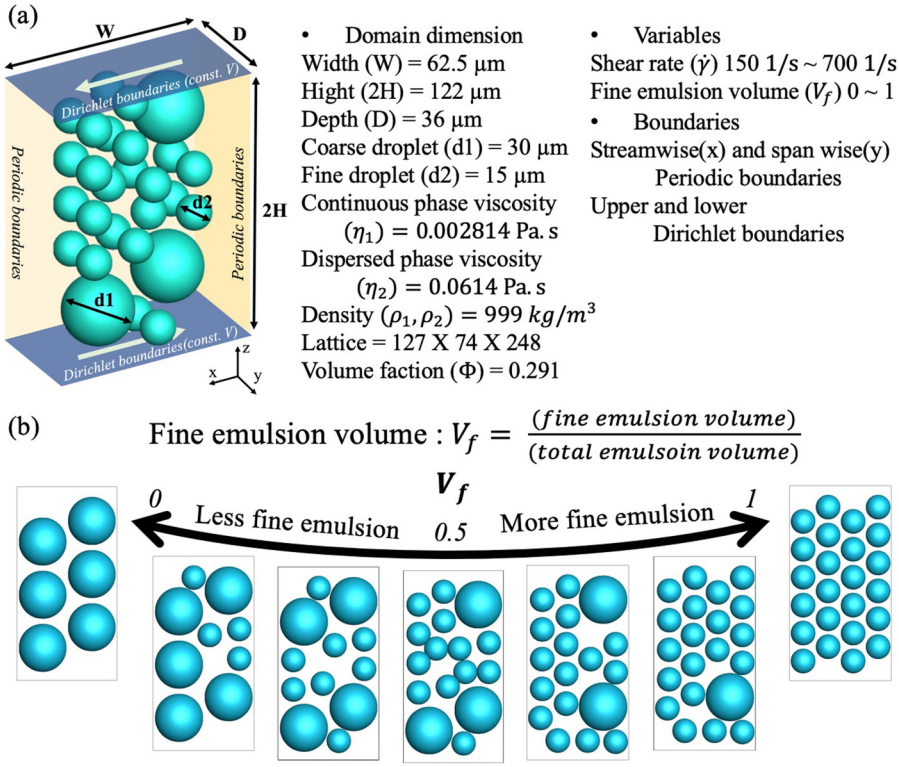

FIG. 4. (a) Emulsion droplet and boundary conditions and (b) droplet fine emulsion volume. $V_f = 0$ consists of 6 coarse droplets and $V_f = 1$ consists of 48 fine droplets.

convection-diffusion equation:[25]

$$\partial_t \Gamma + \nabla_s \cdot (u_s \Gamma) + k \Gamma u_n = D_s \nabla_s^2 \Gamma, \tag{13}$$

where Γ is the surfactant concentration; the velocity components are divided into surface and normal velocity (u_s and u_n, respectively); and D_s is the surfactant diffusivity. These parameters were calculated using the molecular dynamics (MD) simulation proposed by Choi *et al.*[26] The expression $\partial_t \Gamma$ is the regional surfactant concentration related to time; $\nabla_s \cdot (u_s \Gamma)$ is the convection term associated with u_s; and $k \Gamma u_n$ is the interfacial curvature k associated with u_n. The right-hand side $(D_s \nabla_s^2 \Gamma)$ is the diffusion term.

We used the hopscotch explicit finite difference method to solve Eq. (13)[15] and coupled it with the Gunstensen LBM.[16]

TABLE I. Numerical cases used to investigate mixed emulsion relative viscosity.

Shear rate (s^{-1})	Fine emulsion volume range (V_f)
150 200 300 500 700	0, 0.17, 0.33, 0.5, 0.67, 0.83, 1

The surfactant concentration in this model tends to locally exceed the critical micellar concentration (CMC), which was prevented by applying a concentration limit.

Figure 4(a) shows the simulation domain and boundary conditions for the bimodal emulsion. The domain has width = W, height = 2H, and depth = D. Fine and coarse emulsions were modeled as homogenous size according to the experimentally measured Sauter mean diameter. Therefore, droplet size distributions were classified into two sizes using the coarse and fine droplet diameters, d1 and d2, respectively. Viscosity of the continuous phase, η_1, disperse phase, η_2, and the volume fraction, ϕ, of the dispersed phase were the same as those used in the experiment. Densities of the two phases were also the same and the surfactant concentration was represented as Γ.

Figure 4(b) shows bimodal emulsion based on the number of fine and coarse droplets. The volume of the coarse droplets is 8 times that of the fine droplets. Table I shows mixed emulsion cases for different shear rates and V_f.

III. RESULTS AND DISCUSSION

A. Emulsion droplet size and viscosity as V_f

Figure 5 shows microscopic images of the droplets in the solution and the subsequent estimated volume distributions, which are typically normal due to the bulk stirring method

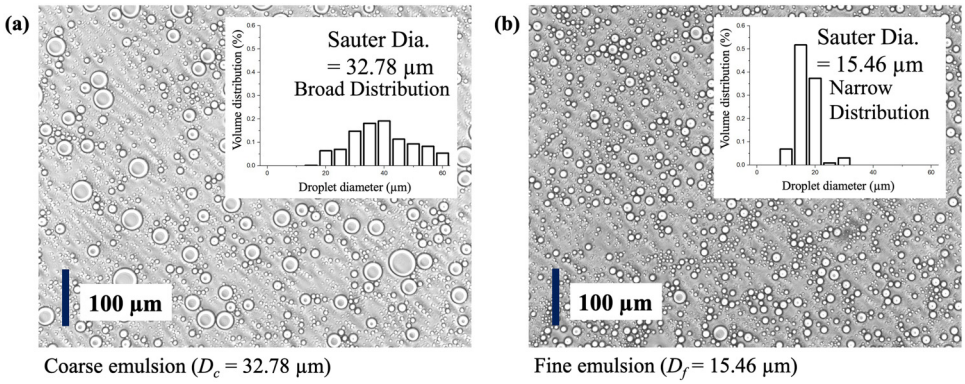

FIG. 5. Phase contrast images for (a) coarse and (b) fine emulsions prior to solutions mixture. Insets are the size distributions obtained from ImageJ. These solutions were used in the experiments.

employed. Coarse and fine emulsions correspond to $V_f = 0$ and 1, respectively, as shown in Fig. 2. The Sauter mean diameter for coarse emulsion is two times larger ($D_c = 32.78\,\mu m$) than that of the fine emulsion ($D_f = 15.46\,\mu m$), and hence the fine emulsion had a significantly narrower volume distribution. The two emulsion solutions were mixed on a volume basis as shown in Fig. 2 and the viscosities measured for the seven mixtures.

Figure 6 compares flow viscosity. Fine emulsion shear thinning is more significant than that for the coarse emulsions, with the $V_f = 0.17$ exhibiting the lowest viscosity. The viscosity difference increases as the shear rate increases.

B. Gunstensen LBM simulation

To study bimodal emulsion rheology at the microscopic level, their relative viscosities were evaluated in a numerical model, which was validated by comparing with the experimental data, as shown in Fig. 7. The fine emulsion system employed produced narrow size distribution emulsions [Fig. 5(b)] with an average droplet size $D = 15.46\,\mu m$, similar to that used in the simulation ($D = 15\,\mu m$). The shear rate was between 150 and 700 s^{-1}, and the simulation shows close similarity with experiment for high shear rates.

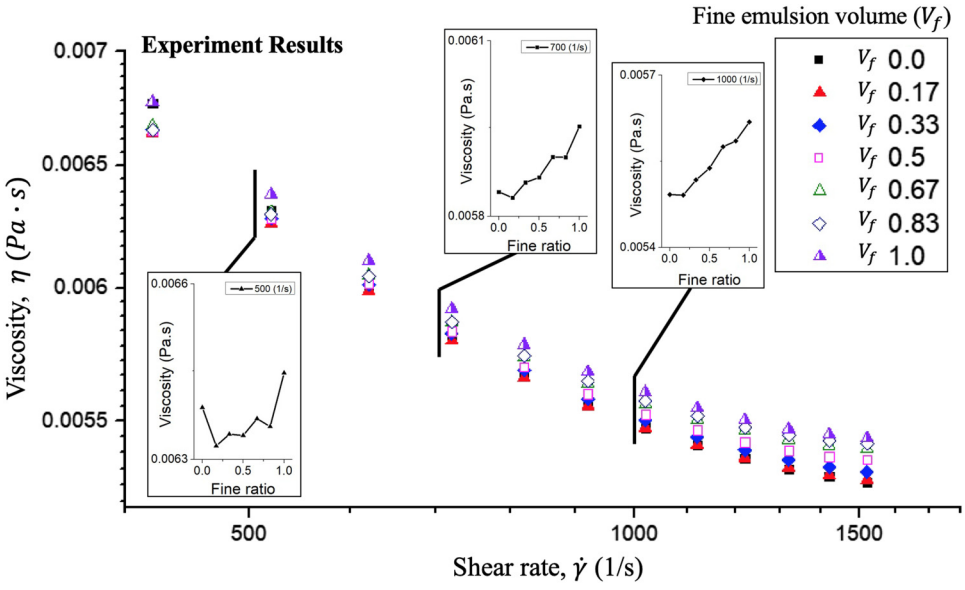

FIG. 6. Experimentally measured emulsion viscosity and the shear rate from the rheometer flow test. Insets show viscosity for specific shear rates.

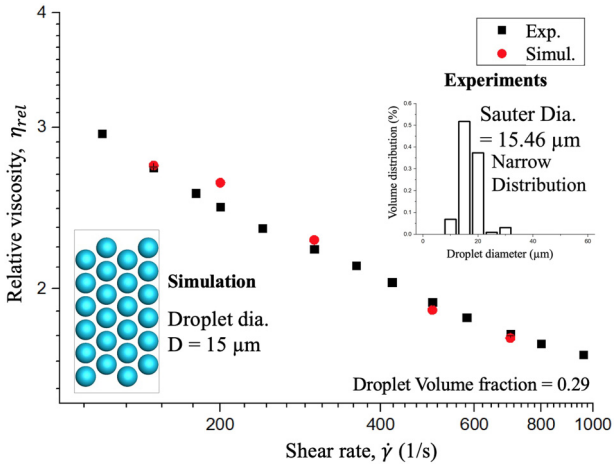

FIG. 7. Numerical simulation validation against experimental data.

C. Shear rate dependent viscosity

The fine emulsion volume can directly affect relative viscosity. Consider the ratio between effective and continuous phase fluid viscosities, $\eta_{rel} = \eta_{eff}/\eta_{fluid}$. The two emulsions have various interfacial interactions, related to droplet size effects, and relative viscosity under simple shear flow can be expressed as

$$\eta_{rel} = \frac{2H}{|V|WD}\sum\frac{\partial u}{\partial z}, \tag{14}$$

where H, D, W, and V are the respective domain height, depth, width, and velocity, as shown in Fig. 4(a). Z direction velocity gradients were evaluated on the upper and lower nodes in adjacent layers, and the time evolution of the viscosity trends was similar to our previous study.[27] Therefore, relative viscosity was compared in the steady-state phase.

Generally, oil-in-water emulsions show non-Newtonian behavior (shear-thinning), and many previous studies have detailed this behavior, such as the Cross model by Howe *et al.*[28]

$$\eta(\dot{\gamma}) = \eta_\infty + \frac{\eta_0 - \eta_\infty}{1 + (k\dot{\gamma})^n}, \tag{15}$$

where η_∞ and η_0 are viscosities at infinite and zero shear rates, respectively; k is the time constant; and n is the shear-thinning index. Figure 8 compares the measured and Cross model relative viscosities. The model predicted $n = 0.72$–0.95 and was consistent with the measured results, and the viscosity trends from Pal *et al.*[4–7]

Figure 9 shows shear stress effects on the mixed emulsions. Shear thinning (the viscosity difference between shear rates) becomes trivial at low V_f. The current data exhibit similar results to Pal *et al.*'s [29] high concentration model when shear rate = 200 s^{-1}, i.e., where $V_f = 0.17$ has the lowest relative viscosity.

D. Averaged droplet deformation and peeling effects

Figure 10 shows that shear flow induces droplet deformation and shear stress changes on the surface. Droplet deformation due to shear flow changes periodicity and peeling due to shear stress occurs over time as the degree of droplet interaction. To explain this interaction, interfacial droplet area rate (A_r) and the peeling effect (interfacial shear stress related) were analyzed.

The interfacial droplet area rate (A_r) describes the uneven droplet deformation as follows:

$$A_r = \frac{A_{max} - A_{init}}{t_{max}A_{init}}, \tag{16}$$

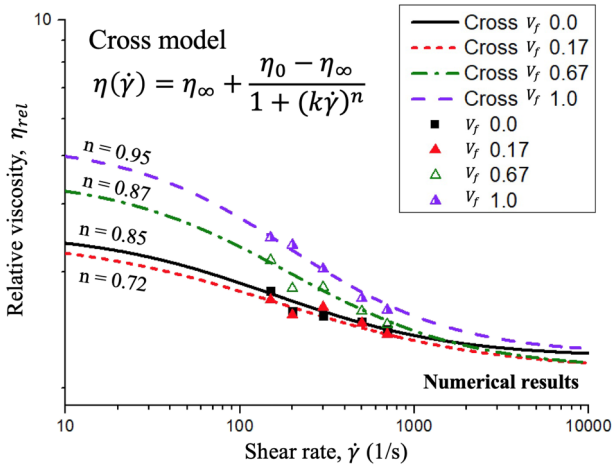

FIG. 8. Relative viscosity and the shear rate from numerical simulations compared with the Cross model outcomes [see Eq. (15)].

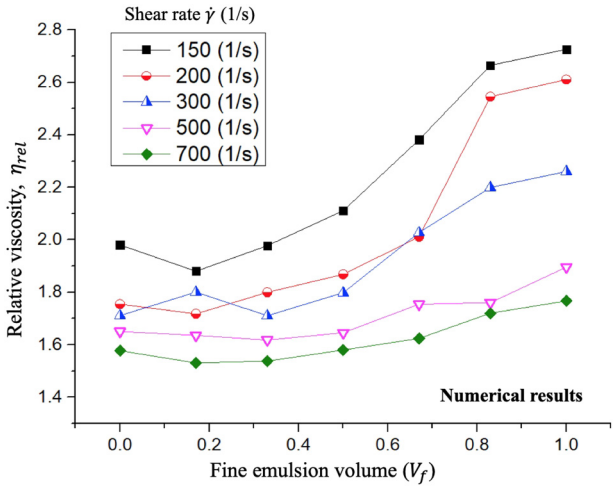

FIG. 9. Numerical simulation for relative viscosities, evaluated from average steady-state phase along the shear rate.

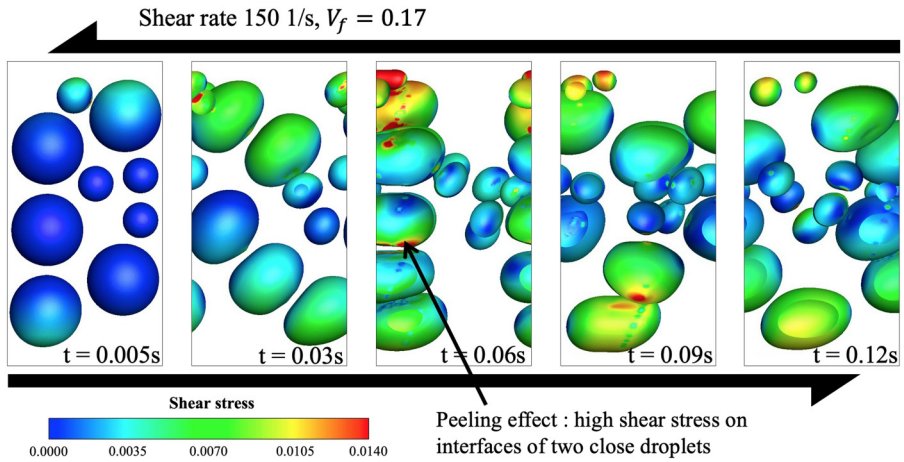

FIG. 10. Numerical simulation for droplet deformation: V_f = 0.17, shear rate = 150 s^{-1}. Droplets were deformed into elliptical shapes with close contact due to shear flow. Droplet contour exhibited surface shear stress, with maximum deformation at approximately 0.06 s. Peeling effects due to contact are also shown.

where A_{max} and A_{init} are the maximum and initial droplet surface area, respectively; and t_{max} is the time step.

Figure 11 shows the relationship between A_r and the normalized surface shear stress with V_f to analyze peeling effect. A_r was obtained when droplet deformation was maximum because the droplets tended to deform and recover when passing through the steady-state phase. Therefore, A_r represents the system flow adoptability. For a monodisperse system, adoptability is purely determined by the droplet size, whereas for a bimodal dispersion, the presence of a small number of small droplets (V_f = 0.17) exhibited significantly higher flow adoptability.

High shear stress at the contact point between droplets can be represented by the peeling effect as proposed by Kondaraju *et al.*[27] to droplet breakup relationships in the aggregate state. The sum of the surface velocity gradients at

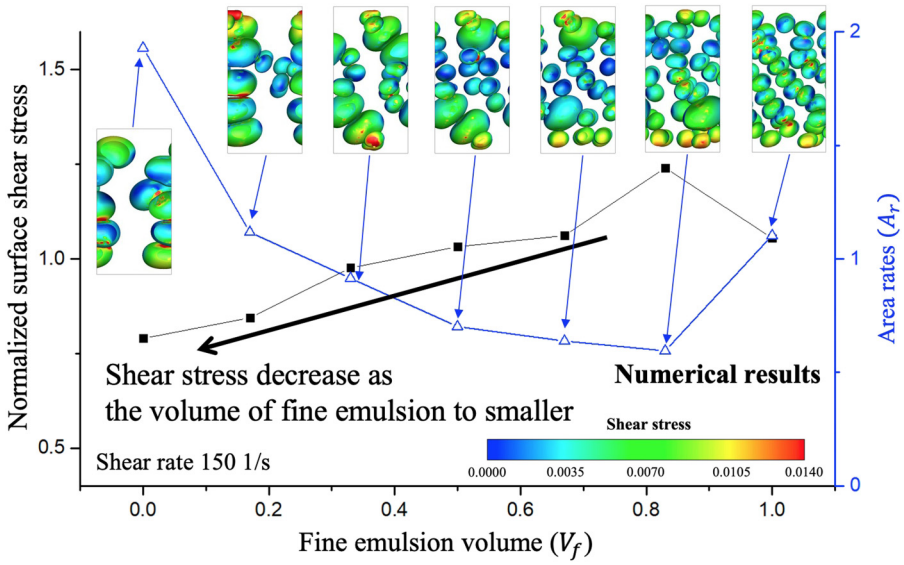

FIG. 11. Numerical simulations for interfacial droplet area (A_r) and surface shear stress for V_f. Insets show typical deformed droplets and surface shear stress contours at t_{max}. Open triangles are normalized surface shear stress for the mixed emulsion in the steady-state region. Both values were normalized to 1.0 and simulated at constant shear rate $\dot{\gamma} = 150\ s^{-1}$.

each node was used for the surface shear stress. However, this surface shear stress changes with time. Thus, we took a time normalize in the steady-state region. The normalized surface shear stress temporally and spatially proves the interaction between individual droplets. The normalized surface shear stress in the steady-state region was dependent on V_f, where the flow disturbance increased with increasing shear stress and *vice versa*. Therefore, reducing V_f will distribute the shear force more evenly on the droplets.

IV. CONCLUSION

This study compared experimental shear flow viscosity and rheological LBM simulations to investigate bimodal distribution emulsion colloidal properties. We presented rheological analysis for dilute emulsion solutions that are difficult to identify experimentally. Experimental results confirmed the relative viscosity correlation with bimodal distribution emulsion. The simulation model provided micro-scale analysis of emulsion properties including relative viscosity, droplet deformation, and surface shear stress.

A mixture of fine and coarse emulsions was analyzed, and mixtures containing a small amount of fine emulsions were found to have a lower relative viscosity and shear thinning due to droplet deformation and surface shear stress. Flow adoptability was the primary cause for low viscosity in the bimodal emulsion system.

The limitation of this study is droplet size homogeneity. Practically, even monodisperse solutions contain various emulsion droplet sizes. If this criterion was met, the shear thinning tendency and the relative viscosity in the simulation would have been similar with those in the experiment. Future work will consider the size design and the droplet number to fit a normal distribution rather than a monodispersed system.

ACKNOWLEDGMENTS

This work was supported by the National Research Foundation of Korea (NRF) Grant funded by the Korean Government (MSIP) (No. 2015R1A5A1037668).

REFERENCES

[1]M. Li, C. Liu, C. Liang, C. Liu, and J. Li, J. Dispers. Sci. Technol. **35**, 397 (2014).
[2]V. Castel, A. C. Rubiolo, and C. R. Carrara, Food Hydrocoll. **63**, 170 (2017).
[3]Y. Yuan, Z. L. Wan, S. W. Yin, Z. Teng, X. Q. Yang, J. R. Qi, and X. Y. Wang, Food Hydrocoll. **31**, 85 (2013).
[4]R. Pal, AIChE J. **42**, 3181 (1996).
[5]R. Pal, Food Hydrocoll. **20**, 997 (2006).
[6]R. Pal, Colloids Surf. A Physicochem. Eng. Asp. **137**, 275 (1998).
[7]R. Pal, Ind. Eng. Chem. Res. **39**, 4933 (2000).
[8]N. Bremond, A. R. Thiam, and J. Bibette, Phys. Rev. Lett. **100**, 1 (2008).
[9]J. D. Martin, J. N. Marhefka, K. B. Migler, and S. D. Hudson, Adv. Mater. **23**, 426 (2011).
[10]R. D'Apolito, A. Perazzo, M. D'Antuono, V. Preziosi, G. Tomaiuolo, R. Miller, and S. Guido, Langmuir **34**, 4991 (2018).
[11]H. Leba, A. Cameirao, J. M. Herri, M. Darbouret, J. L. Peytavy, and P. Glénat, Chem. Eng. Sci. **65**, 1185 (2010).
[12]M. Koroleva, A. Tokarev, and E. Yurtov, Colloids Surf. A Physicochem. Eng. Asp. **481**, 237 (2015).
[13]Y. Zhang, Y. Liu, X. Wang, Z. Li, and Y. Shen, J. Dispers. Sci. Technol. **36**, 259 (2015).
[14]V. Cristini, J. Bławzdziewicz, and M. Loewenberg, Phys. Fluids **10**, 1781 (1998).
[15]H. Farhat, F. Celiker, T. Singh, and J. S. Lee, Soft Matter **7**, 1968 (2011).
[16]A. K. Gunstensen, D. H. Rothman, S. S. Zaleski, and G. Zanetti, Phys. Rev. A **43**, 4320 (1991).
[17]J. Boyd, C. Parkinson, and P. Sherman, J. Colloid Interface Sci. **41**, 359 (1972).
[18]S. W. Hasan, M. T. Ghannam, and N. Esmail, Fuel **89**, 1095 (2010).
[19]R. Chanamai and D. J. McClements, Colloids Surf. A Physicochem. Eng. Asp. **172**, 79 (2000).
[20]I. Halliday, A. P. Hollis, and C. M. Care, Phys. Rev. E Stat. Nonlin. Soft Matter Phys. **76**, 1 (2007).
[21]U. D'Ortona, D. Salin, M. Cieplak, R. B. Rybka, and J. R. Banavar, Phys. Rev. E **51**, 3718 (1995).
[22]S. V. Lishchuk, C. M. Care, and I. Halliday, Phys. Rev. E **67**, 036701 (2003).
[23]Z. Guo, C. Zheng, and B. Shi, Phys. Rev. E **65**, 046308 (2002).
[24]S. P. Lyu, T. D. Jones, F. S. Bates, and C. W. Macosko, Macromolecules **35**, 7845 (2002).
[25]H. A. Stone, Phy. Fluids A: Fluid Dyn. **2**, 111 (1990).
[26]S. Bin Choi, H. M. Yoon, and J. S. Lee, Biomicrofluidics **8**, 052104 (2014).
[27]S. Kondaraju, H. Farhat, and J. S. Lee, Soft Matter **8**, 1374 (2012).
[28]A. M. Howe, A. Clarke, and T. H. Whitesides, Langmuir **13**, 2617 (1997).
[29]R. Pal, Chem. Eng. J. **67**, 37 (1997).